Use of UWB Impulse Radio Technology in In-Car Communications: Power Limits and Optimization

Tamás István Krébesz, *Member, IEEE*, Géza Kolumbán, *Fellow, IEEE*, Chi K. Tse, *Fellow, IEEE*, Francis C. M. Lau, *Senior Member, IEEE*, and Hairong Dong, *Senior Member, IEEE*

***Abstract*—In-car wireless data communications systems require a short-range unlicensed radio communications technology that causes a very low level of interference in the other, already deployed radio links and networks, offers low and medium data rate, can reuse the already occupied radio-frequency (RF) bands, and assures low probability of message collisions. Ultrawide band (UWB) impulse radio employs RF pulses with very short duration to carry the information; consequently, it is an optimal candidate for the in-car wireless communications and intravehicular wireless sensor networks. Data rate and shape of RF carrier pulse determine the performance of a UWB radio link. To limit the interference caused, the maximum power radiated by an UWB device is restricted by the Federal Communications Commission (FCC) in the U.S. Introducing a new mathematical model and starting from the FCC regulations, analytical expressions for the calculation of FCC power limits are derived here. It is shown that the low- and high-rate UWB impulse radio systems are peak and average power limited, respectively. The relationship between the mathematical model and the parameters of an UWB carrier pulse used in a built UWB radio is established. The performances of RF carrier pulses known from the literature are evaluated and compared. All expressions derived are verified by measurements.**

***Index Terms*—Federal Communications Commission (FCC) compliance of ultrawide band (UWB) impulse radio (IR), intravehicular communications, UWB IR communications systems.**

Manuscript received June 13, 2016; revised October 9, 2016 and December 12, 2016; accepted December 27, 2016. Date of publication January 4, 2017; date of current version July 14, 2017. This work was supported by the Pázmány Péter Catholic University under Grant KAP16-71005-1.1-ITK, Grant KAP16-73020-3.6-ITK, and Grant KAP16-75004-5.2-ITK. The work of T. I. Krébesz was supported by the ARTEMIS JU and the Hungarian National Research, Development and Innovation Fund in the framework of the R5-COP project. The collaboration of Hungarian and Chinese researchers was supported in part by the Chinese State Administration of Foreign Experts Affairs Agency in the framework of the High-end Foreign Experts Recruitment Program. The review of this paper was coordinated by Dr. D. W. Matolak.

T. I. Krébesz is with the Department of Measurement and Information Systems, Budapest University of Technology and Economics, Budapest 1111, Hungary (e-mail: krebesz@mit.bme.hu).

G. Kolumbán is with the Faculty of Information Technology and Bionics, Pázmány Péter Catholic University, Budapest 1088, Hungary, and also with the School of Engineering, Edith Cowan University, Joondalup WA 6027, Australia (e-mail: kolumban@itk.ppke.hu).

C. K. Tse and F. C. M. Lau are with the Department of Electronic and Information Engineering, The Hong Kong Polytechnic University, Hong Kong (e-mail: encktse@polyu.edu.hk; encmlau@polyu.edu.hk).

H. Dong is with the State Key Laboratory of Rail Traffic Control and Safety, Beijing Jiaotong University, Beijing 100044, China (e-mail: hrdong@bjtu.edu.cn).

Digital Object Identifier 10.1109/TVT.2017.2647849

I. Introduction

THERE are many applications in vehicle engineering from tire pressure monitoring [1] to intravehicle ranging [2] where wireless data communications technology has to be used. The theoretical studies and measurements performed in real application environments have shown that the propagation conditions are very severe in the in-car radio communications because the radio channel suffers from multipath and its parameters are time variant [3]–[5].

In addition to the severe channel conditions, in-car wireless data communications systems have to meet special application requirements: 1) Compared to the conventional solutions, a short-range radio communications technology is required, which is suitable for unlicensed operation and can work in *ad hoc* networks; 2) the already occupied radio frequency (RF) bands have to be reused, however, only a very low-level of interference can be caused in the other, already deployed radio links and networks; and 3) low probability of message collision has to be assured.

Ultrawide band impulse radio (UWB IR) uses RF pulses with very short duration, typically in the order of a nanosecond, to carry the digital information [6]–[9]. The energy of radiated UWB IR signal is spread almost uniformly over an ultrawide frequency band, consequently, if the power spectral density is kept low enough, then the UWB IR signal will not cause a significant interference in the already deployed narrow-band radio links sharing the same frequency band.

The interior of a vehicle is an inherently dense multipath data communications environment. The narrow pulses with low duty cycle and the UWB feature of UWB IR communications assure robust operation in intravehicular applications [10] and can provide high resistance against narrow-band interferences caused by conventional communications systems [11]. The extremely short pulse durations keep the probability of message collision very low even in an *ad hoc* network. These properties make UWB IR technology an optimal candidate for in-car wireless communications and vehicular wireless sensor networks (VWSNs) [12].

To limit the interference to other radio links, the maximum power level radiated by an UWB device is restricted by the Federal Communications Commission (FCC) in the U.S. [13]. By now the FCC regulations have been accepted and adopted worldwide.

UWB IR communications technology has become a hot research topic. An IEEE 802 Standard for wireless personal and local area networks (WPANs/WLANs) exploiting UWB IR technology was published in 2007. Since then a lot of amendments and revisions have been approved, the latest version of IEEE 802.15.4 Standard was approved in 2015 [14].

Many UWB IR radio devices have been built for WPAN/WLAN applications and field tests have been carried out. The field tests have revealed that the FCC-compliant UWB IR devices have only a few-meter radio range [15], consequently, they can only be used in wireless in-car communications, VWSNs and body area networks.

This contribution gives a theoretical reasoning of the short UWB IR radio coverage. It investigates the feasibility of FCC-compliant UWB impulse radio links by deriving closed-form theoretical expressions. It is shown that the FCC regulations allow to radiate only such a low power that strictly limits the application areas of UWB IR technology to those ones where only a few-meter radio range is required.

To perform the investigations, two basic characteristics of an UWB IR transmitter have to be fixed: 1) the power radiated and 2) the shape of radiated waveform.

The FCC regulations give the power limits on an UWB radiator but they say nothing about the shape of the UWB IR waveform. Different shapes can be used by the different manufacturers but interoperability has to be assured.

Neither an industrial standard nor an IEEE Standard is available for the UWB IR-based in-car communications. Because the IEEE 802.15.4 Standard satisfies all requirements of in-car communications and VWSN applications, the IEEE Std. 802.15.4 of 2015 is considered here.

Section II surveys the relevant parts of the FCC regulations and IEEE 802.15.4 Standard. The victim narrow-band receiver is modeled by a bandpass filter in the FCC regulations and the interference caused by an UWB radiator is specified at the output of that filter. To limit all kinds of interferences, the FCC regulations define two bandpass filters, and the peak and average power levels of UWB interference are measured at the output of those filters.

Section III surveys the IEEE Standard-compliant UWB carrier pulse envelopes published up to now and establishes a unified mathematical model which 1) can be applied to any kind of UWB IR waveforms and 2) is suitable for the derivation of closed-form expressions for both FCC power limits. The unified mathematical model relies on the fact that the bandwidth of an UWB IR pulse is always much larger than that of the two FCC bandpass filters. Therefore, the UWB carrier pulse can be considered as an impulse excitation to the FCC bandpass filters and the FCC power limits can be determined from the impulse responses of the FCC filters. The unified model assures that the theory derived here can be applied to any UWB IR carrier.

Section IV derives analytical expressions for the FCC peak and average power limits. The peak power limit is calculated in the time domain while the average power limit is determined from the Parseval's relation. To get closed-form expressions, piecewise linear approximations of Jacobi theta functions are used. The validity of approximations have been verified by measurements.

The importance of the analysis method developed here goes beyond the study of UWB IR systems because it can be used everywhere, where 1) the response of a bandpass filter to a train of arbitrary RF pulses has to be determined or 2) the peak and average power levels of a pulsed RF signal are measured by a spectrum analyzer. Until now, only heuristic equations have been available for this purpose which made the measurement of pulsed RF signals by a spectrum analyzer inaccurate [16], [17].

Section V interprets the theoretical expressions obtained and determines the maximum peak level of generalized UWB IR carrier pulse envelope allowed by the FCC regulations as a function of the pulse repetition frequency. The result obtained confirms theoretically two phenomena observed in built UWB IR systems: 1) The low- and high-rate UWB IR links are peak and average power limited, respectively [18], and 2) the radio coverage of FCC-compliant UWB IR systems is limited in a few meters by the very low energy allowed to transmit one bit information.

The shape of UWB IR carrier pulse envelope and the data rate are free design parameters. Section V determines the optimum data rate where the maximum radio coverage is achieved and compares the performances of different RF carrier pulses known from the literature.

Section VI draws the conclusion.

II. Restrictions on UWB IR Carriers

Short-range unlicensed radio communications technology developed for in-car and VWSN applications has to comply with the FCC regulations [13]. The FCC regulations restrict the maximum allowable level of interference caused by an UWB radiator to other radio systems but say nothing about the UWB system parameters. Another, a vehicle specific standard is required to define the channel bandwidths and frequencies, shape of UWB IR carrier pulse and data rate. The duty of vehicle specific standard is to assure interoperability among the UWB radio devices produced by different manufacturers.

A vehicle-specific UWB IR standard has not yet been elaborated but an IEEE standard where the UWB IR technology can be used to implement the physical layer (PHY) is available. Depending on the UWB IR carrier pulse repetition frequency two versions of UWB PHY are specified in the IEEE Std. 802.15.4-2015 [14], the high-rate pulse (HRP) and low-rate pulse (LRP) PHYs. However, the IEEE Standard provides a detailed specification only for the HRP UWB IR system.

Since the specification given in the IEEE Std. 802.15.4-2015 for the HRP UWB IR physical layer satisfies the requirements of in-car and VWSN applications, that IEEE Standard will be used here to define the missing UWB PHY parameters.

To simplify our terminology, the two restrictions on UWB IR carriers are referred to as FCC regulations and IEEE Standard in the rest of this paper.

A. FCC Limits on Radiated UWB IR Signals

Restrictions on UWB IR signals were published by FCC in 2002 [13]. To limit the interference to other radio systems, the peak and average values of equivalent isotropically radiated power (EIRP) transmitted by an UWB device are limited.

1) "There is a limit on the *peak* level of the emissions contained within a 50-MHz bandwidth centered on the frequency at which the highest radiated emission occurs $\cdots$ That limit is 0-dBm EIRP."
2) The *average* "radiated emissions $\cdots$ shall not exceed" $-$ 41.3-dBm EIRP "when measured using a resolution bandwidth of 1 MHz" over the frequency band of 3.1–10.6 GHz.
   "The RMS average measurement is based on the use of a spectrum analyzer with a resolution bandwidth of 1 MHz, an RMS detector, and a 1-ms or less averaging time."

The former and latter restrictions are referred to as FCC *peak* and *average* power limits in the rest of our investigations. A built UWB transmitter has to comply with both restrictions.

EIRP is the product of the power supplied to the antenna input and the antenna gain relative to an isotropic antenna. To avoid confusion, EIRP and the output power of the UWB transmitter will not be distinguished here. Because EIRP is limited by the FCC regulations, the equations derived here always refer to the radiated power, i.e., EIRP.

The 50-MHz and 1-MHz RF bandpass filters are referred to as FCC bandpass filters in the rest of this contribution.

B. Requirements of IEEE Standard

The IEEE Standard gives the specification for the PHY of an UWB IR transceiver [14]. Altogether 16 RF UWB channels and four different bandwidths are defined where the 3-dB RF bandwidth of an HRP UWB channel can be set to one of the following values: 499.2, 1081.6, 1331.2, and 1354.97 MHz. The transmit spectrum mask is also specified for each HRP UWB channel and the 10-dB RF bandwidth of transmit spectrum mask exceeds considerably the channel bandwidth given in the HRP UWB PHY band allocation table. To avoid confusion, the RF channel bandwidths defined in the HRP UWB PHY band allocation table will be used here to identify the different implementations.

The implementation of the UWB pulse generator is the key issue in the design of UWB transceivers. To give a high level of freedom to circuit designer, the IEEE HRP UWB Standard does not specify the exact shape of the UWB carrier. Any kind of UWB pulses can be used provided that

1) it satisfies the FCC regulations;
2) it obeys the transmit spectrum mask of IEEE Standard;
3) its correlation with a reference pulse exceeds a specified level.

UWB transceivers using different UWB carriers have to operate in the same network. To assure interoperability, the IEEE Standard defines a *reference pulse* and specifies the properties of cross correlation between the envelope of an UWB pulse used by an IEEE 802.15.4-compliant HRP UWB IR transceiver and the reference pulse

$$r(t) = \frac{4\beta}{\pi\sqrt{T_p}} \frac{\cos\left[(1+\beta)\frac{\pi t}{T_p}\right] + \frac{\sin\left[(1-\beta)\frac{\pi t}{T_p}\right]}{4\beta\frac{t}{T_p}}}{1-\left(4\beta\frac{t}{T_p}\right)^2}. \quad (1)$$

The reference pulse is a square-root raised cosine (SRRC) function, where T_p denotes the channel-dependent pulse duration specified in the IEEE Standard and $\beta = 0.5$ is the roll-off factor.

The normalized cross correlation of the reference pulse (1) with the envelope of an IEEE 802.15.4-compliant UWB IR carrier pulse has to meet the following two requirements:

1) magnitude of its main lobe shall be at least 0.8 over a channel-dependent duration T_w specified in the IEEE Standard;
2) peak value of the magnitude of all other side lobes shall be no greater than 0.3.

A short remark on notation: many times the same letter combination is used as both an abbreviation and a variable. The abbreviations are given in capital roman fonts, while the variables are typed in italics. If an abbreviation is also used as a variable or appears in a variable, then it is given in capital roman font in this contribution. For example, SRRC stands for square-root raised cosine, however, it is also a part of the variable $r^{[\mathrm{SRRC}]}(t)$ in (2) of Section III-B.

III. Mathematical Model

The UWB circuit and system designers need the following two basic parameters:

1) the peak level A of the envelope of the UWB pulse generated at the transmitter;
2) the energy E_p carried by one UWB IR pulse.

To improve the radio coverage, the IEEE Standard allows to use more than one UWB IR pulse to transmit one bit of information [14]. This idea has been also exploited in VWSN applications [19]. This is why a distinction is made here between the energy carried by one UWB IR pulse and the energy per bit. The latter one is given by $E_b = M \times E_p$ where M denotes the number of pulses used to transmit one bit of information and E_p is the energy carried by one UWB IR pulse. Note, A determines the required output voltage swing to be assured at the UWB transmitter, while E_b determines the attainable radio coverage.

This paper provides the relationship among these UWB parameters and the FCC regulations. Only those UWB pulses, which satisfy the IEEE HRP UWB Standard are considered here. To derive analytical expressions, first the FCC regulations have to be interpreted and a unified mathematical model valid for each UWB IR carrier pulse has to be elaborated.

A. Interpretation of FCC Regulations

As discussed in Section II-A, the FCC regulations rely on a bandpass filter with two different bandwidths: 50 MHz for the peak and 1 MHz for the average power limit measurements.

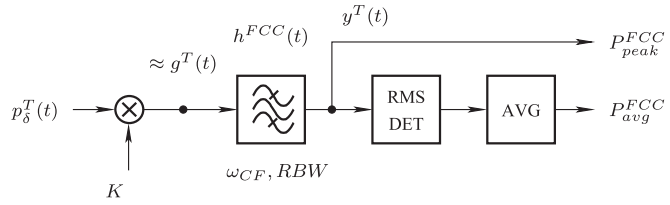

Fig. 1. Unified mathematical model for the interpretation of FCC regulations.

The FCC regulations not only give the power limits but also provide instructions on how those limits have to be measured.

Let $P^{\mathrm{FCC}}_{\mathrm{peak}}$ and $P^{\mathrm{FCC}}_{\mathrm{avg}}$ denote the FCC peak and average power limits, respectively. The mathematical model constructed from the FCC regulations is depicted in Fig. 1, where $g^T(t)$ denotes the train of UWB IR carrier pulses to be tested, $h^{\mathrm{FCC}}(t)$ is the impulse response of the FCC bandpass filter, ω_{CF} and RBW give the center frequency and resolution bandwidth, respectively, of that filter. The periodicity of UWB IR signals is reflected by the upper index T. Note, the FCC peak limit is determined from the peak value of the FCC filter output $y^T(t)$, while the measurement of the FCC average limit needs an RMS detector (RMS DET) and averaging (AVG).

The rate at which an IEEE 802.15.4-compliant UWB IR transmitter emits pulses is given by the pulse repetition frequency (PRF), its maximum value is limited to 499.2 MHz [14]. The FCC regulations have been elaborated to limit the interference caused by the UWB radiators. They specify neither the shape nor the number of UWB IR pulses used to carry one bit of information. The PRF is the only parameter that has to be considered during the derivation of FCC power limits. Note that $T = 1/\mathrm{PRF}$.

Because the exact shape of the UWB IR carrier is not specified, many different UWB IR carrier pulses have been proposed in the literature [8], [20]–[24]. To cover all of these UWB IR carrier pulses, a unified mathematical model is developed first. In the unified model, depicted in Fig. 1, the train $g^T(t)$ of UWB IR carrier pulses emitted by the built UWB transmitter under test is approximated by the product of a train $p^T_\delta(t)$ of Dirac delta functions and a pulse-shape-dependent weighting factor K. The validity of this approximation follows from the fact that, according to the FCC regulations, the 10-dB RF bandwidth of a UWB signal has to be at least 500 MHz, consequently, the bandwidth of an UWB IR signal is always much greater than that of the FCC bandpass filter. If so then, over the frequency band where the frequency response of the FCC filter is not negligible, the spectrum of $g^T(t)$ can be substituted by the spectrum of a train of weighted Dirac delta functions. Therefore, the UWB pulse can be considered as an impulse excitation to the FCC filter and the FCC regulations are directly related to the impulse response of the FCC filter. For all details on UWB IR signal decomposition and the validity of this approximation refer to Section III-C.

B. IEEE 802.15.4-Compliant UWB IR Carrier Pulses

A number of functions have been proposed to implement the *envelope* of an UWB IR carrier. Many of them do not satisfy the IEEE Standard. This section surveys the IEEE 802.15.4-compliant UWB IR pulses known from the literature.

The use of an *SRRC function*, that is, the reference pulse as the envelope of UWB IR carrier gives the trivial solution. The peak level A of envelope appears at $t = 0$ and the SRRC UWB IR pulse is obtained from (1) as

$$r^{[\mathrm{SRRC}]}(t) = A\frac{4\beta}{\beta(4-\pi)+\pi} \times \frac{\cos\left[(1+\beta)\frac{\pi t}{T_p}\right] + \frac{\sin\left[(1-\beta)\frac{\pi t}{T_p}\right]}{4\beta\frac{t}{T_p}}}{1-\left(4\beta\frac{t}{T_p}\right)^2}. \quad (2)$$

The reason, which prevents the use of the reference pulse in its original form is that it cannot be generated by simple CMOS microwave circuits.

The *Gaussian pulse* [8] is often considered as an UWB envelope in theoretical investigations because it and its derivatives are convenient to be expressed and manipulated mathematically. The Gaussian pulse takes the form

$$p^{[\mathrm{GAUSS}]}(t) = A\exp\left(-\frac{t^2}{2u_B^2}\right) \quad (3)$$

where A, as before, is the peak level of envelope and u_B is determined by the 10-dB RF bandwidth $2f_B$ of the UWB carrier

$$u_B = \frac{1}{2\pi f_B\sqrt{\log_{10}(e)}}.$$

Researchers at Massachusetts Institute of Technology (MIT) approximated the Gaussian pulse in their built UWB transmitter by a *tanh pulse* [20]

$$p^{[\mathrm{TANH}]}(t) = 0.545A\left[1-\tanh\left(\frac{4.4}{3.99u_B}|t|-1.2\right)\right]. \quad (4)$$

In an alternative MIT solution, the response of a second-order low-pass filter to a square wave input was used as pulse envelope [18]

$$p^{[\mathrm{FILT}]}(t) = A\times\begin{cases}0, & \text{if } t<0\\ f(t), & \text{if } 0\le t<\tau\\ f(t)-f(t-\tau), & \text{if } t\ge\tau\end{cases} \quad (5)$$

where τ denotes the pulsewidth and

$$f(t) = 1-\frac{1}{0.6}\exp\left(-3.2\frac{t}{\tau}\right)\sin\left[2.4\frac{t}{\tau}+\arccos(0.8)\right]. \quad (6)$$

The constants in (4) and (6) had been determined in such a way that the mean squared error measured between the UWB IR pulse envelopes proposed by MIT and the Gaussian one was minimized. As before, A denotes the peak level of envelopes in (4) and (5).

The aforementioned equations give only the envelope of an UWB IR carrier pulse. To get the UWB IR carrier, these signals are up-converted into the microwave frequency region by a mixer

$$g^{[\cdot]}(t) = p^{[\cdot]}(t)\cos(\omega_C t) \quad (7)$$

where the upper index $[\cdot]$ identifies the type of envelope and $\omega_C = 2\pi f_C$ is the center frequency of the UWB radio channel.

C. Unified Model for UWB IR Carrier Pulses

As shown on the left side of Fig. 1, the train of UWB IR carrier pulses is approximated by a periodic impulse train

$$g^T(t) = g^{[\cdot],T}(t) \approx K p_\delta^T(t) \tag{8}$$

where the weighting factor K depends on the type of envelope. Its values for the IEEE 802.15.4-compliant UWB IR carrier pulses are determined in this section.

To prove the validity of approximation (8), the spectra of $Kp_\delta^T(t)$ and $g^{[\cdot],T}(t)$ have to be compared. If the two spectra are equal to each other over the frequency band where the magnitude of frequency response of the FCC bandpass filter is not negligible, then approximation (8) holds.

Spectrum of an impulse train is given in the literature [25]

$$\mathcal{F}\left\{Kp_\delta^T(t)\right\} = \frac{K}{T}\sum_{k=-\infty}^{\infty}\delta\left(f-\frac{k}{T}\right). \tag{9}$$

Next, the spectra of the trains of UWB carrier pulses have to be determined.

Consider an UWB IR carrier where the envelope is a Gaussian pulse. Then, one period of the UWB IR carrier pulse train is obtained by substituting (3) into (7)

$$g^{[\text{GAUSS}]}(t) = A\exp\left(-\frac{t^2}{2u_B^2}\right)\cos(\omega_C t).$$

The Fourier series coefficients of a periodic signal can be determined from the Fourier transform of one period [25]. The Gaussian envelope decays rapidly as a function of time, consequently, $g^{[\text{GAUSS}]}(t)$ is negligible outside the period time T and the Fourier transform of *one period* is obtained as

$$\begin{aligned}\mathcal{F}\left\{g^{[\text{GAUSS}]}(t)\right\} &= A\frac{\sqrt{2\pi}\,u_B}{2}\left[\exp\left(-2\left[\pi u_B(f-f_C)\right]^2\right)\right.\\ &\quad\left.+\ \exp\left(-2\left[\pi u_B(f+f_C)\right]^2\right)\right].\end{aligned} \tag{10}$$

The Fourier series coefficients of the *periodic* $g^{[\text{GAUSS}],T}$ can be determined from (10) and the spectrum of the train of UWB IR carrier pulses is obtained from its Fourier series expansion as

$$\begin{aligned}\mathcal{F}\left\{g^{[\text{GAUSS}],T}(t)\right\} &= A\frac{\sqrt{2\pi}\,u_B}{2T}\\ &\quad\times\sum_{k=-\infty}^{\infty}\left[\exp\left(-2\left[\pi u_B\left(\frac{k}{T}-f_C\right)\right]^2\right)\delta\left(f-\frac{k}{T}\right)\right.\\ &\quad\left.+\ \exp\left(-2\left[\pi u_B\left(\frac{k}{T}+f_C\right)\right]^2\right)\delta\left(f-\frac{k}{T}\right)\right].\end{aligned} \tag{11}$$

Approximation (8) holds if the following two conditions are met:

1) spectra of (9) and (11) are identical at
$$f = \frac{k}{T} \approx f_C \tag{12}$$
2) variation in $\mathcal{F}\left\{g^{[\text{GAUSS}],T}(t)\right\}$ is negligible in the frequency band of interest.

The weighting factor K is obtained from condition 1 by substituting (12) into (9) and (11). The second term in the right-hand side (RHS) square bracket of (11) becomes almost zero when it is evaluated about f_C. Neglecting this term and equalling (9) and (11) at $f \approx f_C$, K is obtained for the Gaussian envelope as

$$K = \frac{\sqrt{2\pi}\,u_B}{2}A.$$

To verify condition 2, the maximum variation in the spectrum lines of the Gaussian UWB IR carrier pulse train given by (11) has to be determined over the frequency range where the frequency response of the 50-MHz FCC bandpass filter is not negligible.

The FCC regulations are checked by a spectrum analyzer where the FCC bandpass filters are implemented by the RF bandpass filter of the spectrum analyzer. Almost all spectrum analyzers use a Gaussian filter to set the resolution bandwidth [16], [26]. The attenuation of a Gaussian filter increases rapidly as a function of detuning, for example, the attenuation of a 50-MHz bandwidth Gaussian filter at 64.44-MHz detuning is 20 dB.

Due to this high attenuation, the contribution of the spectrum lines to $P_{\text{peak}}^{\text{FCC}}$ and $P_{\text{avg}}^{\text{FCC}}$ at the FCC filter output can be neglected beyond 64.44-MHz detuning. Consequently, the maximum variation in $\mathcal{F}\left\{g^{[\text{GAUSS}],T}(t)\right\}$, denoted by $\text{var}_{\max}$, has to be evaluated up to this value of detuning. For a Gaussian UWB IR carrier, $\text{var}_{\max} = 0.67$ dB and it causes only a negligible error in the FCC power limits to be derived later, in Section IV.

Table I gives $\text{var}_{\max}$ for the IEEE 802.15.4-compliant UWB IR carrier pulses surveyed in Section III-B. Note, $\text{var}_{\max}$ is negligible in all cases.

The value of weighting factor K depends on the type of envelope. For the IEEE 802.15.4-compliant UWB IR carrier pulses, the weighting factors and the energies carried by one UWB IR pulse are given in Table I as a function of the peak level A of envelope. The FCC regulations set an upper limit on K from which both the required voltage swing $2A$ at the UWB transmitter output and the energy E_p carried by one UWB IR pulse can be determined. The relationship between K and the FCC regulations is established in the next section.

Table I also gives the equations that express the energy carried by one pulse as a function of the peak level of envelope. The UWB waveform is measured over Z_0, the characteristic impedance of the UWB system. These equations will be used later for the calculations of UWB IR system parameters.

IV. Derivation of Peak and Average Power Limits

Section III-C has proved that an UWB IR signal can be considered as an impulse excitation to the FCC bandpass filter. The FCC limits are derived from $y^T(t)$ of Fig. 1, that is, from the output of the FCC filter.

TABLE I
PARAMETERS OF THE IEEE 802.15.4A-COMPLIANT UWB IR CARRIERS

[SRRC]	$\text{var}_{\max}$	0.10 dB
	K	$\frac{T_p\,\pi}{2\beta(4-\pi)+2\pi}A$
	E_p	$\frac{T_p}{[(1-\beta)+4\beta/\pi]^2}\frac{A^2}{2Z_0}$
[GAUSS]	$\text{var}_{\max}$	0.67 dB
	K	$\frac{\sqrt{2\pi}u_B}{2}A$
	E_p	$\sqrt{\pi}u_B\frac{A^2}{2Z_0}$
[TANH]	$\text{var}_{\max}$	0.73 dB
	K	$\frac{3.99u_B\,\ln(1+\mathrm{e}^{2.4})}{4.4[1+\tanh(1.2)]}A$
	E_p	$\frac{3.99u_B\,[2\ln(\mathrm{e}^{2.4}+1)-\tanh(1.2)-1]}{2.2[1+\tanh(1.2)]^2}\frac{A^2}{2Z_0}$
[FILT]	$\text{var}_{\max}$	0.15 dB
	K	$\frac{\tau}{2-\frac{2}{0.6}\mathrm{e}^{-3.2}\sin[2.4+\arccos(0.8)]}A$
	E_p	$\approx 0.7464\tau\frac{A^2}{2Z_0}$

According to the FCC regulations, the FCC peak power limit can be measured, while the average power limit has to be measured by a spectrum analyzer. Let both $P_{\text{avg}}^{\text{FCC}}$ and $P_{\text{peak}}^{\text{FCC}}$ be measured by a spectrum analyzer. Therefore, in our investigations, the FCC filters are Gaussian bandpass filters with an impulse response

$$h^{\text{FCC}}(t)=\frac{2}{\sqrt{2\pi}\,\lambda}\exp\left[-\frac{(t-\tau_{\text{CF}})^2}{2\lambda^2}\right]\cos\left[\omega_{\text{CF}}(t-\tau_{\text{CF}})\right] \tag{13}$$

where τ_{CF} is the total delay of the spectrum analyzer, and

$$\lambda=\frac{\sqrt{2\ln\sqrt{2}}}{\pi\ \text{RBW}}\ . \tag{14}$$

As shown in Fig. 1, ω_{CF} and RBW are the center frequency and the 3-dB bandwidth, respectively, of the FCC bandpass filter. Note, two different values of λ will be used later because different RBW s have to be used to calculate the FCC peak and average power limits. Also note, that ω_C may differ from ω_{CF} since according to the FCC regulations the power limits have to be checked at the frequency of highest radiation.

The mathematical model of Fig. 1 shows that the response of the FCC filter to *a single isolated UWB IR carrier pulse* $g(t)$ is

$$y(t)=\frac{2K}{\sqrt{2\pi}\,\lambda}\exp\left[-\frac{(t-\tau_{\text{CF}})^2}{2\lambda^2}\right]\cos\left[\omega_{\text{CF}}(t-\tau_{\text{CF}})\right]. \tag{15}$$

However, an UWB radiator transmits a sequence of UWB pulses and the FCC filter output becomes a periodic signal with a period T. This periodicity is reflected by the upper index T in $y^T(t)$. Since the FCC filter is a linear time-invariant circuit, the superposition theorem can be applied and $y^T(t)$ can be expressed as a sum of delayed and weighted impulse responses of the FCC filter. This periodic output is shown in Fig. 2, where not only $y^T(t)$ but also its envelope is plotted by a dashed curve. In the case shown in the figure PRF $\ll$ RBW, consequently, the impulse responses to the individual UWB pulses do not overlap one another. The effect of overlapping will be taken into account later in Sections IV-A and IV-B where $y^T(t)$ will be used to derive both the FCC peak and average power limits.

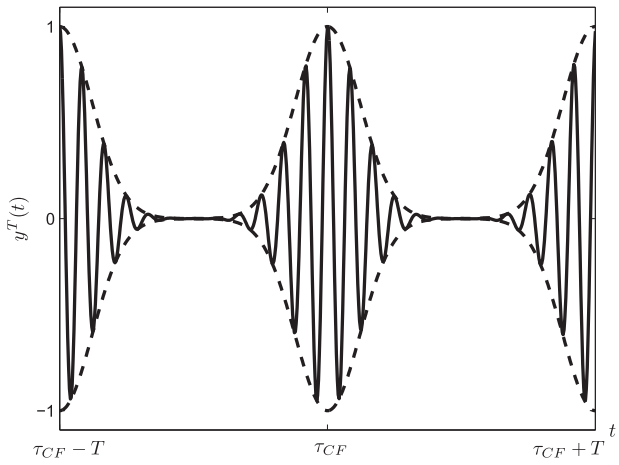

Fig. 2. Periodic output $y^T(t)$ of the FCC filter when PRF $\ll$ RBW and overlapping does not occur. Solid and dashed curves show the FCC filter output and its envelope, respectively.

A. FCC Peak Power Limit

The FCC peak power limit restricts the peak output power of the 50-MHz FCC bandpass filter to 0 dBm. The center frequency of FCC bandpass filter has to be set to the frequency at which the highest radiated emission occurs.

The FCC peak power limit can be calculated from the peak voltage of the FCC filter output in the time domain. To get the peak power, only the peak voltage has to be expressed and the calculation can be simplified by considering only the envelope of the FCC filter output

$$y(t)\le y_{\text{env}}(t)=\frac{2K}{\sqrt{2\pi}\,\lambda_{50}}\exp\left[-\frac{(t-\tau_{\text{CF}})^2}{2\lambda_{50}^2}\right]$$

where λ_{50} is obtained from (14) by substituting RBW $=$ 50 MHz.

When PRF $\ll$ RBW overlapping does not occur. This situation is shown in Fig. 3, where the Gaussian waveform depicted is the envelope of the bandpass RF signal measured at the FCC filter output (see dashed curve in Fig. 2). Note, the envelope $y_{\text{env}}^T(t)$ is a periodic waveform with the period time $T=1/\text{PRF}$ and its peaks appear at $\tau_{\text{CF}}\pm nT$, $n=0,1,2,\ldots$.

In the general case, overlapping occurs. In Fig. 4, the dashed, dotted and dash-dotted curves give the envelopes of FCC filter responses to three consecutive individual UWB pulses, while the resultant output envelope is shown by the solid curve. Only three individual responses are plotted in the figure, the presence of the other ones is marked by three dots on both sides. A few important conclusions can be drawn, which are as follows.

1) Since the worst-case situation has to be considered and the superposition theorem is applicable to the FCC filter,

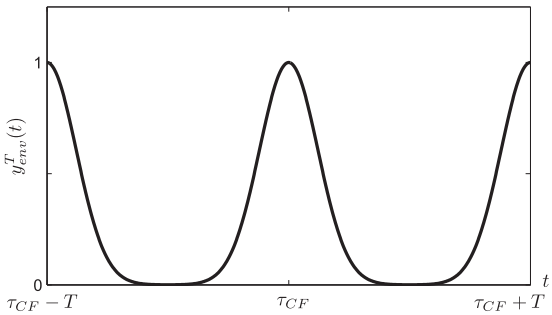

Fig. 3. Envelope of the FCC filter output when PRF $\ll$ RBW. Note that the FCC filter outputs generated by the individual UWB pulses are separated completely. The time elapsed between two consecutive peaks is equal to $T = 1/\text{PRF}$.

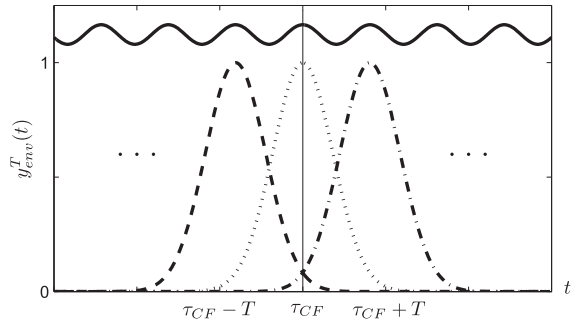

Fig. 4. Envelope of the FCC filter output when PRF $>$ RBW. Dashed, dotted, and dash-dotted curves give the envelopes of FCC filter responses to three consecutive individual UWB pulses, while the solid curve gives the resultant output envelope. Note that the FCC filter outputs generated by the individual UWB pulses well overlap one another.

the individual responses have to be summed and the peaks increase in value with increasing overlapping.

2) The peaks of the FCC filter output appear at $\tau_{\text{CF}} \pm nT, n = 0, 1, 2, \ldots$.

Let the peak power be calculated at $t = \tau_{\text{CF}}$. Then, the peak value of the FCC filter output is

$$\begin{aligned} y_{\text{env}}^T(\tau_{\text{CF}}) &= \tfrac{2K}{\sqrt{2\pi}\,\lambda_{50}} \left(\cdots + \exp\left[-\tfrac{(T)^2}{2\lambda_{50}^2}\right] + 1 \right. \\ &\quad \left. + \exp\left[-\tfrac{(-T)^2}{2\lambda_{50}^2}\right] + \cdots \right) \\ &= \tfrac{2K}{\sqrt{2\pi}\,\lambda_{50}} \textstyle\sum_{n=-\infty}^{\infty} \exp\left[-\tfrac{(nT)^2}{2\lambda_{50}^2}\right] \end{aligned} \tag{16}$$

where the three terms in the bracket give, from the left to the right, respectively, the contributions of the dashed, dotted, and dash-dotted curves plotted in Fig. 4.

Exploiting the symmetry of the exponential terms, we put (16) into the form

$$y_{\text{env}}^T(\tau_{\text{CF}}) = \frac{2K}{\sqrt{2\pi}\lambda_{50}} \left(1 + 2\sum_{n=1}^{\infty} \exp\left[-\frac{(nT)^2}{2\lambda_{50}^2}\right] \right). \tag{17}$$

To get a closed-form expression for the FCC peak power limit, the sum of exponentials in (17) has to be determined.

The Jacobi theta functions are defined in mathematics. One of them takes the form in the notation of Whittaker and Watson [27] as

$$\vartheta_3(z, q) = 1 + 2\sum_{n=1}^{\infty} q^{n^2} \cos(2nz) \tag{18}$$

where q and z denote the nome and argument, respectively.

A comparison of (17) and (18) shows that if we substitute $z = 0$ and $q = \exp\left(-\frac{T^2}{2\lambda_{50}^2}\right) = \exp\left[-\frac{1}{2(\lambda_{50}\text{PRF})^2}\right]$ in (18), then the peak voltage of FCC filter output can be expressed by the Jacobi theta function as

$$y_{\text{env}}^T(\tau_{\text{CF}}) = \frac{2K}{\sqrt{2\pi}\lambda_{50}}\, \vartheta_3\left(0, \exp\left[-\frac{1}{2(\lambda_{50}\text{PRF})^2}\right]\right). \tag{19}$$

Although an analytical expression is not available for the calculation of $\vartheta_3(z, q)$, its value can be determined numerically [28].

The result of numerical calculation is shown in Fig. 5 where the Jacobi theta function is plotted for $z = 0$ as a function of the product of λ_{50}PRF. Note, for $z = 0$, the Jacobi theta function can be approximated by a piecewise linear function with a negligible error

$$\begin{aligned} &\vartheta_3\left(0, \lambda_{50}\text{PRF}\right) \\ &\quad = \begin{cases} 1, & \text{if } \lambda_{50}\text{PRF} \le 1/\sqrt{2\pi} \\ \sqrt{2\pi}\,\lambda_{50}\text{PRF}, & \text{otherwise.} \end{cases} \end{aligned} \tag{20}$$

Using this approximation, all equations are available to express the peak power at the FCC filter output in the analytical form.

Let the FCC bandpass filter be terminated by Z_0. As shown by Figs. 3 and 4, the peak voltage at the FCC filter output appears at $t = \tau_{\text{CF}} \pm nT$, $n = 0, 1, 2, \ldots$ and the peak power is obtained as

$$P_{\text{peak}} = \frac{\left[y_{\text{env}}^T(\tau_{\text{CF}})\right]^2}{Z_0}. \tag{21}$$

Substituting (19) into (21) and taking into account the piecewise linear approximation of (20), the peak power at the FCC bandpass filter output is obtained as

$$\begin{aligned} P_{\text{peak}} &= \frac{2}{\pi\lambda_{50}^2}\,\frac{K^2}{Z_0} \\ &\quad \times \begin{cases} 1, & \text{if } \lambda_{50}\text{PRF} \le 1/\sqrt{2\pi} \\ 2\pi(\lambda_{50}\text{PRF})^2, & \text{otherwise.} \end{cases} \end{aligned} \tag{22}$$

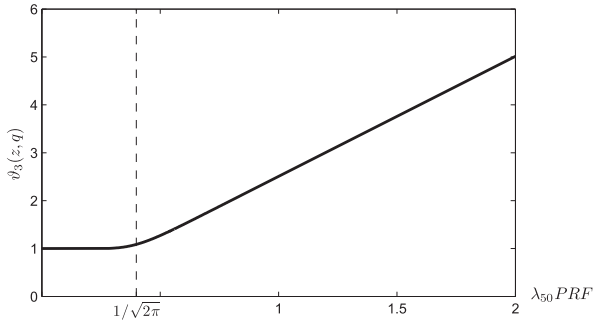

Fig. 5. Jacobi theta function for $z = 0$ and $q = \exp\left[-\frac{1}{2(\lambda_{50}\text{PRF})^2}\right]$.

The FCC peak power limit restricts P_{peak} to 1 mW. Equation (22) establishes the relationship between P_{peak} and the UWB pulse-shape-dependent weighting factor K introduced in the unified mathematical model of Fig. 1. Then, the peak level of an IEEE 802.15.4-compliant UWB envelope can be calculated from K, the equations required are given in Table I.

B. FCC Average Power Limit

Checking of the FCC average power limit requires a spectrum analyzer with a resolution bandwidth of 1 MHz, an RMS detector, and a 1-ms or less averaging time. The block diagram of measurement setup is shown in Fig. 1.

The output of the FCC bandpass filter is a periodic signal that can be represented by its Fourier series. Since the Parseval's Relation establishes the relationship between the average power of a periodic signal and the absolute values of its Fourier coefficients, the FCC average power limit is derived here from the Fourier coefficients of $y^T(t)$. The steps of investigation are as follows.

1) First, the Fourier coefficients of $Kp_\delta^T(t)$ are calculated.
2) Then, those of FCC filter output are derived.
3) The average power measured at the FCC filter output is determined from the Parseval's relation.

The FCC filter is driven by a sequence of weighted Dirac delta functions $Kp_\delta(t)$. The Fourier coefficients of this periodic excitation $Kp_\delta^T(t)$ can be calculated from the Fourier transform of one period [25] as

$$a_k = \frac{1}{T}\mathcal{F}\left\{Kp_\delta(t)\right\}\Big|_{f=\frac{k}{T}} = \frac{K}{T}\,\delta_{ik}$$

where δ_{ik} is the Kronecker delta function, $i = fT$ and $k = 0, \pm1, \pm2, \ldots$.

The Fourier coefficients of the periodic FCC filter output $y^T(t)$ are obtained as

$$\begin{aligned} b_k &= H^{\text{FCC}}(f)\Big|_{f=\frac{k}{T}}\, a_k = \frac{K}{T}\,H^{\text{FCC}}(f)\,\delta_{(fT)k} \\ &= \frac{K}{T}\,H^{\text{FCC}}\left(\frac{k}{T}\right) \end{aligned} \tag{23}$$

where the frequency response of the Gaussian FCC filter is retrieved by taking the Fourier transform of (13)

$$\begin{aligned} H^{\text{FCC}}(f) = \big[&\exp\left(-2[\pi\lambda_1(f+f_{\text{CF}})]^2\right) \\ &+\ \exp\left(-2[\pi\lambda_1(f-f_{\text{CF}})]^2\right)\big]\exp(-j2\pi f\tau_{\text{CF}}). \end{aligned} \tag{24}$$

Recall, λ_1 is obtained from (14) by substituting RBW $= 1$ MHz.

As shown by (23), except a weighting factor K/T, the Fourier coefficients b_k are determined by the frequency response of the Gaussian FCC bandpass filter.

The average power at the FCC filter output can be calculated from the Parseval's relation

$$P_{\text{avg}} = \frac{1}{Z_0}\sum_{k=-\infty}^{\infty}|b_k|^2 = \frac{1}{Z_0}\left(\frac{K}{T}\right)^2\sum_{k=-\infty}^{\infty}\left|H^{\text{FCC}}\left(\frac{k}{T}\right)\right|^2. \tag{25}$$

The next step is the determination of the sum on the RHS in closed form. Recall, the FCC average power limit has to be checked by a narrow-band bandpass filter, where

1) $|H^{\text{FCC}}(0)| = 0$;
2) $f_{\text{CF}} \gg \text{RBW} = 1$ MHz, that is, overlapping between the two exponential terms, given in the bracket on the RHS in (24), does not occur.

Considering these conditions and substituting (24) into (25), we get

$$P_{\text{avg}} = \frac{4}{Z_0}\left(\frac{K}{T}\right)^2\sum_{k=1}^{\infty}\exp\left(-4\left[\pi\lambda_1\left(\frac{k}{T}-f_{\text{CF}}\right)\right]^2\right). \tag{26}$$

Always the worst-case scenario has to be considered in the FCC regulations. In general $k/T \approx f_{\text{CF}}$ but the maximum of (26) is obtained when f_{CF} is an entire multiple of PRF $= 1/T$. Let a new variable $n = k - f_{\text{CF}}T$ be introduced in (26); then, we get

$$P_{\text{avg}} = \frac{4K^2}{Z_0T^2}\sum_{n=1-f_{\text{CF}}T}^{\infty}\exp\left[-4\left(\pi\frac{\lambda_1}{T}n\right)^2\right]. \tag{27}$$

The exponential term is an even function of n and it decays very rapidly as a function of n. Therefore, (27) can be well approximated by

$$P_{\text{avg}} = \frac{4K^2}{Z_0T^2}\left(1+2\sum_{n=1}^{\infty}\exp\left[-4\left(\pi\frac{\lambda_1}{T}n\right)^2\right]\right). \tag{28}$$

A comparison of (28) and (18) shows that the term in the bracket on the RHS of (28) is equal to the Jacobi theta function with $z = 0$ and $q = \exp[-4(\pi\lambda_1\text{PRF})^2]$. As shown in Section IV-A, this Jacobi theta function can be approximated by a piecewise linear function with a negligible error and the average power is obtained as

$$\begin{aligned} P_{\text{avg}} &= 4\,(\text{PRF})^2\,\frac{K^2}{Z_0} \\ &\times\begin{cases} 1/(\sqrt{4\pi}\,\lambda_1\text{PRF}), & \text{if } \lambda_1\text{PRF} \le 1/\sqrt{4\pi} \\ 1, & \text{otherwise.} \end{cases} \end{aligned} \tag{29}$$

The FCC average power limit restricts P_{avg} to -41.3 dBm. Equation (29) establishes the relationship between P_{avg} and the UWB pulse-shape-dependent weighting factor K.

Since an UWB IR transmitter has to obey both FCC limits, an UWB IR system may be either peak [see (22)] or average [refer to (29)] power limited depending on PRF $= 1/T$. This issue will be discussed later in Section V.

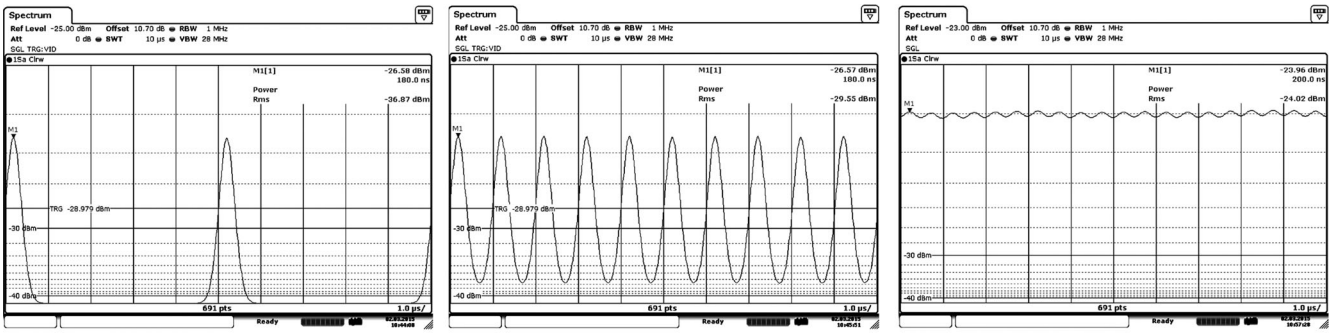

Fig. 6. Measurement of the envelope of $y^T(t)$ in dBm for three cases: (a) PRF $= 200$ kHz and overlapping does not occur, (b) PRF $= 1$ MHz and overlapping among the Gaussian pulses just begins, and (c) PRF $= 2$ MHz and a considerable overlapping is present. In each measurement RBW has been set to 1 MHz.

C. Verification of FCC Limits by Measurements

Equations derived for the FCC peak and average power limits have been verified by measurements, where

1) an NI PXIe-based I/Q signal generator has been used to generate the train $g^{[\cdot],T}(t)$ of UWB IR carrier pulses;
2) an R&S FSV3 signal and spectrum analyzer (SSA) has been used to check the waveform $y^T(t)$ at the FCC filter output and to measure $P_{\rm peak}$ and $P_{\rm avg}$ given by (22) and (29), respectively.

To cancel all measurement errors, the microwave test setup has been carefully calibrated prior to the verification.

Recall, both FCC peak and average power limits have been derived from the envelope of $y^T(t)$ in Sections IV-A and IV-B. The envelope is a train of Gaussian pulses, where, depending on the PRF to RBW ratio, overlapping among the consecutive pulses does not or does occur. Figs. 3 and 4 show the calculated waveforms for PRF $<$ RBW (no overlapping) and PRF $>$ RBW (overlapping), respectively. First, these waveforms have been checked by measurements.

To verify $y^T(t)$, a train of UWB IR carrier pulses generated by the I/Q signal generator has been fed into the spectrum analyzer. In *zero span mode* the SSA implements the FCC bandpass filter depicted in Fig. 1 and the envelope of FCC filter output can be recovered by the built-in RMS detector.

The measured envelopes for three different PRF s are shown in Fig. 6 where RBW $= 1$ MHz and the peak envelope power (PEP) is returned by the marker. The most important conclusions are as follows.

1) *Fig. 6(a):* Since PRF $= 200$ kHz $<$ RBW, overlapping does not occur. PEP $= -26.58$ dBm.
2) *Fig. 6(b):* PRF $= 1$ MHz $=$ RBW and overlapping among the Gaussian impulses just begins. The low overlapping does not yet increase PEP, its value is -26.57 dBm.
3) *Fig. 6(c):* Since PRF $= 2$ MHz $>$ RBW, a considerable overlapping is present. Overlapping causes a significant increase in PEP, its value is -23.96 dBm.

Fig. 6(a) and (c) corresponds to Figs. 3 and 4, respectively. Identity of corresponding figures validates the model of Fig. 1.

A close look at Fig. 6(c) reveals one more chance for the verification of (22) and (29). Observe, if λPRF is large enough, then a strong overlapping occurs (PRF $\gg$ RBW) and the peak and average power levels become identical at the FCC filter output.

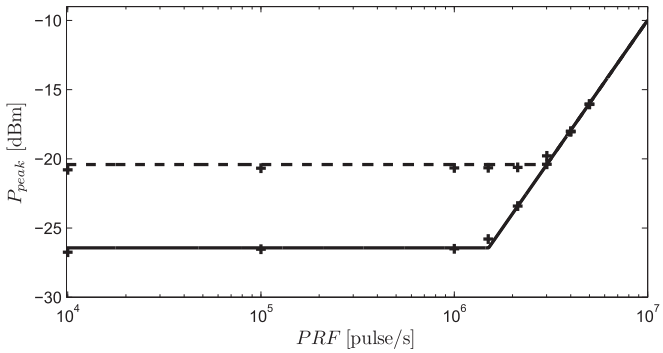

Fig. 7. Peak power at the FCC filter output as a function of PRF. The solid and dashed curves have been predicted from (22) for $\lambda = 265$ ns and $\lambda = 132.5$ ns, respectively, and the "+" marks show the results of measurements.

Note that λ_1PRF is always greater than λ_{50}PRF. Let $\lambda_{50}\text{PRF} \gg 1/\sqrt{2\pi}$ in (22) and (29). Then, as expected

$$P_{\rm peak}\Big|_{\lambda_{50}\text{PRF}\gg 1/\sqrt{2\pi}} = 4\frac{K^2}{Z_0}(\text{PRF})^2 = P_{\rm avg}\Big|_{\lambda_1\text{PRF}\gg 1/\sqrt{4\pi}}. \tag{30}$$

Finally, the expressions derived for the FCC power limits have been verified by measurements. Both $P_{\rm peak}$ and $P_{\rm avg}$ have been calculated and measured for two SSA resolution bandwidths. The values of parameter λ have been set to 265 and 132.5 ns.

Fig. 7 shows the peak power at the FCC bandpass filter output as a function of PRF. The solid and dashed curves have been calculated from (22) for $\lambda = 265$ ns and $\lambda = 132.5$ ns, respectively, and the results measured by the SSA in zero span mode are given by "+" marks. Note, the data predicted from (22) are in an extremely good agreement with the measured data even in the transition region where $\lambda\text{PRF} \approx 1/\sqrt{2\pi}$.

The average power at the FCC bandpass filter output has been measured by the RMS detector and video filter built-in the R&S FSV3 SSA, the averaging time has been set to 1 ms. The average power levels calculated from (29) are plotted by solid and dashed curves for $\lambda = 265$ ns and $\lambda = 132.5$ ns, respectively, in Fig. 8, as a function of PRF and the measured results are shown by "+"

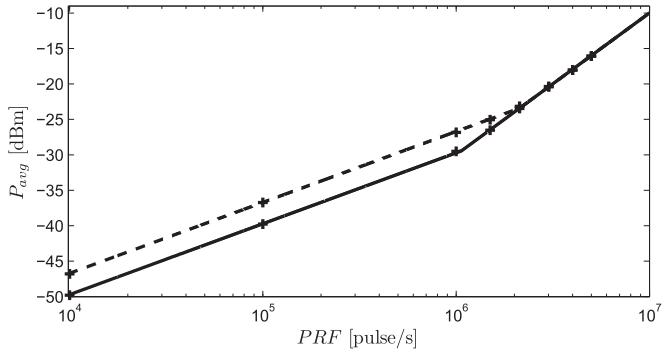

Fig. 8. Average power at the FCC filter output as a function of PRF. The solid and dashed curves have been predicted from (29) for $\lambda = 265$ ns and $\lambda = 132.5$ ns, respectively, and the "+" marks show the results of measurements.

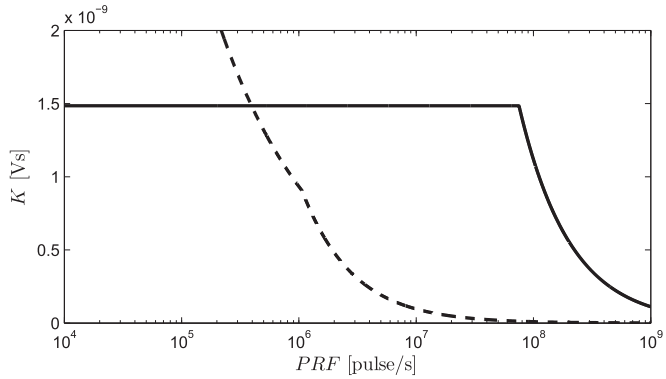

Fig. 9. Maximum allowable value of K as a function of PRF. The FCC peak and average power limits are plotted by solid and dashed curves, respectively.

marks. The extremely good agreement between the predicted and measured data validates the expression derived for the FCC average power limit.

The starting point of overlapping is clearly identified by the breakpoints of both Figs. 7 and 8. The measured results verify that the piecewise linear approximation of the Jacobi theta function is very accurate, even in the transition region.

Equation (30) predicts that both $P_{\rm peak}$ and $P_{\rm avg}$ become independent of λ for large PRF. Merging of curves in Figs. 7 and 8 for large PRF verify this effect predicted theoretically.

Note, the FCC power limits expressed by (22) and (29), later verified by Figs. 7 and 8, have been derived from the UWB pulse-shape-dependent weighting factor K introduced in the unified mathematical model of Fig. 1. Recall, the unified mathematical model is valid for each implemented pulse envelope. The relationship between K and the actual parameters of IEEE 802.15.4-compliant UWB IR carrier pulses will be revealed in the next section.

V. Interpretation of Results and Optimization of UWB IR System Parameters

The FCC regulations have been elaborated to limit the interference caused by an UWB radiator to other radio links. On the other hand, the FCC peak and average power limits determine the following two main UWB system parameters:

1) peak level A of UWB pulse envelope, which specifies the output voltage swing to be assured by the output stage of the UWB transmitter;
2) energy E_p carried by one UWB IR pulse.

The output voltage swing $2A$ determines the supply voltage required, a crucial issue in battery operated applications, while a large radio coverage requires a high $E_b = M \times E_p$.

A. FCC Power Limits and Optimum PRF

The IEEE 802.15.4-compliant UWB IR carrier pulses have been modeled by a periodic impulse train in the unified mathematical model of Section III-C, where the magnitude of one impulse is given by the weighting factor K. Substituting the FCC peak and average power limits into (22) and (29), respectively, the maximum allowable level of K is obtained and plotted in Fig. 9 as a function of pulse repetition frequency. The solid and dashed curves give the FCC peak and average power limits, respectively. Note, the low-rate UWB IR systems are *peak power limited* while high-rate ones are *average power limited*.

The energy carried by one UWB IR pulse is proportional to the square of K. In the optimum case, the UWB IR system simultaneously assures the maximum radio coverage and the highest data rate. If the pulse repetition frequency is a free design parameter, then this optimum system performance is achieved at the crossing point of the solid and dashed curves in Fig. 9. The optimum value of PRF can be expressed analytically from (22) and (29) as

$$\mathrm{PRF}_{\rm opt} = \frac{P_{\rm avg}}{P_{\rm peak}} \frac{\lambda_1}{\lambda_{50}^2} \frac{1}{\sqrt{\pi}} = 394.4 \text{ kpulse/s}\,.$$

Recognize, the optimum value of PRF depends neither on the shape of UWB IR carrier envelope nor on its parameters. It is determined exclusively by the FCC regulations. This conclusion is also valid for Figs. 7–9.

Fig. 9 also reveals why UWB IR technology cannot assure large radio coverage in high-data rate applications. If the data rate is much greater than $\mathrm{PRF}_{\rm opt}$, then K is strongly limited by the FCC average power limit as shown by the dashed curve in Fig. 9.

Note that $\mathrm{PRF} = M \times R_b$, where R_b denotes the data rate to be assured. If $R_b < \mathrm{PRF}_{\rm opt}$, then more than one UWB IR carrier pulse can be used to transmit one bit information and the radio coverage can be increased considerably.

B. Parameters of IEEE 802.15.4-Compliant UWB IR Carriers

The IEEE 802.15.4-compliant UWB IR carrier pulses have been collected in Section III-B. The pulse repetition frequency is fixed by the application and the maximum FCC regulations-compliant value of K is obtained from Fig. 9. Then, the envelope of UWB IR carrier pulse has to be chosen, and finally, the parameters of the IEEE 802.15.4-compliant UWB IR carrier can be calculated from the equations provided in Table I.

The peak level A of UWB IR envelope and energy E_p carried by one UWB IR pulse are shown for the IEEE 802.15.4-compliant UWB IR carrier pulses in Table II for the four HRP UWB channel bandwidths (see the column of RF BW) defined

TABLE II
MAXIMUM PEAK LEVEL OF ENVELOPES AND ENERGY CARRIED BY ONE IEEE 802.15.4-COMPLIANT UWB IR CARRIER PULSE ALLOWED BY THE FCC REGULATIONS

RF BW [MHz]	PRF [pulse/s]	Pulse Param.	Type of UWB IR Pulse Envelope SRRC	GAUSS	TANH	FILT
499.2	10 k	A [V]	1.69	2.24	2.28	1.63
		E_p [pJ]	44	47	46.62	35.91
	394.4 k	A [V]	1.69	2.24	2.28	1.63
		E_p [pJ]	44	47	46.62	35.91
	10 M	A [mV]	10.9	14.5	14.8	10.6
		E_p [fJ]	1.85	1.97	1.96	1.51
1081.6	10 k	A [V]	3.66	4.84	4.94	3.51
		E_p [pJ]	95.52	101.8	101.0	77.4
	394.4 k	A [V]	3.66	4.84	4.94	3.51
		E_p [pJ]	95.52	101.8	101.0	77.4
	10 M	A [mV]	236.9	314	320	227.7
		E_p [fJ]	401.2	427.3	424.2	325
1331.2	10 k	A [V]	4.5	5.96	6.08	4.34
		E_p [pJ]	117.6	125.3	124.3	95.59
	394.4 k	A [V]	4.5	5.96	6.08	4.34
		E_p [pJ]	117.6	125.3	124.3	95.59
	10 M	A [mV]	291.5	386.5	393.8	281.2
		E_p [fJ]	493.8	526.1	522.1	401.5
1354.97	10 k	A [V]	4.58	6.07	6.19	4.43
		E_p [pJ]	119.7	127.5	126.5	97.6
	394.4 k	A [V]	4.58	6.07	6.19	4.43
		E_p [pJ]	119.7	127.5	126.5	97.6
	10 M	A [mV]	296.7	393.4	400.9	287.2
		E_p [fJ]	502.6	535.5	531.5	409.9

The data are given for the four HRP UWB RF channel bandwidths and for three PRFs.

in the IEEE Standard. Three PRFs are considered, among them, as discussed before, $\mathrm{PRF}_{\mathrm{opt}} = 394.4$ kpulse/s assures the optimum system parameters.

Altogether 16 RF HRP UWB channels are defined in the IEEE Standard. Because parameters K, A, and E_p depend only on the FCC regulations and the shape of the UWB IR carrier envelope, the data provided in Table II do not depend on the center frequency of an UWB channel.

Table II reveals the most important inherent characteristics of an FCC regulations-compliant UWB IR radio system, which are as follows.

1) Energy carried by one UWB IR carrier pulse is very low.
2) E_p depends on the RF channel bandwidth: The larger the channel bandwidth, the higher the radio coverage.
3) E_p can be maximized by an appropriate selection of the shape of UWB carrier envelope. However, because of the interoperability requirement, E_p cannot be improved considerably by an appropriate choice of the envelope, the maximum variation in E_p is about 0.9 dB.
4) If PRF exceeds 10 Mpulse/s, then E_p becomes so low that the UWB IR system cannot be used in in-car communications.

These observations reveal why the coverage achieved by the built UWB IR radio systems is very short, much shorter as it was expected. Just for comparison, the energy used to transmit one bit of information in an IEEE 802.15.4-compliant ZigBee application has to be greater than 2 nJ, its typical values in US and Europe are 4 μJ and 500 nJ, respectively. These values considerably exceed E_p allowed by the FCC regulations for the UWB transmitters. Since the radio coverage is determined by the energy per bit, even if more than one UWB IR pulse is used to transmit one bit of information, the extremely low E_b radiated can provide only a very short radio coverage.

VI. CONCLUSION

The radio channels in vehicular applications suffer from dense multipath, frequency selective deep fading, and strong interferers. Under these severe channel conditions, the conventional narrow-band radio communications technologies fail to work, therefore, a brand-new solution is required.

In addition to the severe channel conditions, intravehicular wireless sensor networks and in-car wireless data communications systems have to meet many special requirements: An unlicensed radio communications technology is needed that causes a very low-level of interference in the other, already deployed radio links and networks, can reuse the already occupied RF bands and assures low probability of message collision. The radio devices have to operate in an *ad hoc* manner and the battery operation, that is, the ultralow power consumption, is a must in the majority of applications.

RF pulses with very short duration are used in UWB IR to carry the digital information. Because of their UBW property, the UWB IR radio signals are very robust against multipath fading. The very narrow carrier pulses and the low duty cycle assure a very low probability of message collision and a low power consumption. Hence, UWB IR communications technology offers an optimal solution to vehicular wireless data communications.

The UWB IR communications technology has been elaborated for unlicensed applications, a feature that is a must in the intravehicular applications. The interference caused by an UWB IR transmitter in other radio links is restricted by the FCC regulations, which limit both the peak and average level of UWB emission. Starting from the FCC regulations, analytical expressions have been derived for the calculation of FCC power limits. It has been shown theoretically that the FCC power limits allow to radiate only such a low pulse energy, which restricts the radio coverage of UWB IR systems in a few meters. However, the short radio coverage is not a problem in the intravehicular applications, even more, it is an advantage when the security issues have to be considered.

There are two system parameters that have very strong influence on the performance of every wireless communications system: The data rate and the shape of UWB IR carrier pulse. The analytical expressions derived here for the FCC peak and average power limits prove theoretically that the low- and high-rate UWB IR systems are peak and average power limited, respectively. The crossing point of the two FCC power limits gives the optimum pulse repetition frequency where the maximum radio coverage is achieved. The optimum PRF is 394.4 kpulse/s and if the data rate to be assured is lower than that value, then more than one UWB IR carrier pulse can be used to transmit one bit information. In this manner, the radio coverage of low-rate UWB IR systems can be increased considerably, even it can be controlled in an adaptive manner.

The FCC regulations do not specify the exact shape of the UWB IR carrier waveform. However, some restrictions have to be applied in order to assure interoperability among the UWB IR devices fabricated by the different manufacturers. The actual shape of the UWB carrier determines the peak level of transmitted signal and the energy carried by one UWB pulse. The former and latter give the supply voltage required and the radio coverage attainable, respectively.

The UWB IR carrier waveforms published up to now have been collected and their parameters have been determined. It has been pointed out that the parameters of an UWB IR system cannot be improved considerably by an appropriate choice of the shape of carrier envelope because of the interoperability requirement. Therefore, that shape has to be used, which offers the simplest implementation and best power efficiency.

Exact theoretical analysis of a train of narrow RF pulses has been an unsolved issue in spectrum analysis. The problem appears at high pulse repetition frequency where overlapping occurs in the peak and average power measurements. This paper has shown that the problem of overlapping can be solved by using the Jacobi theta function. The approach presented here can be used not only in the design of UWB IR systems but anywhere in spectrum analysis where the peak and/or average power of pulsed RF signals have to be determined.

The theory and equations developed have been verified by measurements where the UWB IR pulses have been generated by an NI PXIe-based I/Q signal generator and the pulse trains have been measured by an R&S SSA. The extremely good agreement between the results predicted by the analytical expressions and measured in the test bed verifies the theory presented here.

REFERENCES

[1] J. Hidalgo, F. G. Zurbriggen, M. Orefice, and G. C. Vietti, "Wireless link measurement at UWB in a tire sensor system," in *Proc. IEEE Int. Conf. Appl. Electromagn. Commun.*, Dubrovnik, Croatia, Oct. 14–16, 2013, pp. 1–5.

[2] A. Prokes, T. Mikulasek, J. Blumenstein, C. F. Mecklenbrauker, and T. Zemen, "Intra-vehicle ranging in ultra-wide and millimeter wave bands," in *Proc. IEEE Asia Pacific Conf. Wireless Mobile*, Bandung, Indonesia, Aug. 27–29, 2015, pp. 246–250.

[3] I. J. G. Zuazola, J. M. H. Elmirghani, and J. Batchelor, "High-speed ultra-wide band in-car wireless channel measurements," *IET Commun.*, vol. 3, no. 7, pp. 1115–1123, Jul. 2009.

[4] S. Ghamari, G. Tasselli, Y. Guo, C. Robert, C. Botteron, and P.-A. Farine, "Path-loss and car-body-effect characterization for smart tires communications at UWB and ISM bands," in *Proc. IEEE Veh. Technol. Conf.*, Seoul, Korea, May 18–20, 2014, pp. 1–5.

[5] A. Chandra *et al.*, "Frequency-domain in-vehicle UWB channel modeling," *IEEE Trans. Veh. Technol.*, vol. 65, no. 6, pp. 3929–3940, Jun. 2016.

[6] R. A. Scholtz and M. Z. Win, "Impulse radio," in *Wireless Communications, TDMA versus CDMA*, S. G. Glisic and P. A. Leppanen, Eds. New York, NY, USA: Springer-Verlag, 1997, ch. 7, pp. 245–263.

[7] M. Z. Win and R. A. Scholtz, "Impulse radio: How it works," *IEEE Commun. Lett.*, vol. 2, no. 2, pp. 36–38, Feb. 1998.

[8] K. Siwiak and D. McKeown, *Ultra-Wideband Radio Technology*. Chichester, U.K.: Wiley, 2004.

[9] Y. Chao and R. A. Scholtz, "Ultra-wideband transmitted reference systems," *IEEE Trans. Veh. Technol.*, vol. 54, no. 5, pp. 1556–1569, Sep. 2005.

[10] C. U. Bas and S. C. Ergen, "Ultra-wideband channel model for intra-vehicular wireless sensor networks beneath the chassis: From statistical model to simulations," *IEEE Trans. Veh. Technol.*, vol. 62, no. 1, pp. 14–25, Jan. 2013.

[11] X. Cheng and Y. L. Guan, "Narrow-band interference suppression in impulse-radio ultrawideband systems," *IEEE Trans. Veh. Technol.*, vol. 63, no. 7, pp. 3440–3446, Sep. 2014.

[12] R. Liu, S. Herbert, T. H. Loh, and I. J. Wassel, "A study on frequency diversity for intra-vehicular wireless sensor networks (WSNs)," in *Proc. IEEE Veh. Technol. Conf.*, San Francisco, CA, USA, Sep. 5–8, 2011, pp. 1–5.

[13] Federal Communications Commission, *Part 15 of the Commission Rs Rules Regarding Ultra-Wideband Transmission Systems; Subpart F*, FCC–USA. 2016. [Online]. Available: http://hallikainen.com/FccRules/>

[14] *IEEE Standard for Low-Rate Wireless Networks*, LAN/MAN Standards Committee of the IEEE Computer Society, IEEE Std. 802.15.4-2015 (Revision of IEEE Std. 802.15.4-2011), 2015.

[15] K. Maichalernnukul, F. Zheng, and T. Kaiser, "Design and performance of dual-hop MIMO UWB transmission," *IEEE Trans. Veh. Technol.*, vol. 59, no. 6, pp. 2906–2920, Jul. 2010.

[16] *Spectrum Analysis ... Pulsed RF*, Agilent Spectrum Analyzer Series, Application Note 150-2, Agilent Technologies, Palo Alto, CA, USA, May 2005.

[17] G. Bellusci, G. J. M. Janssen, J. Yan, and C. C. J. M. Tiberius, "Performance evaluation of a low-complexity receiver concept for TOA-based ultrawideband ranging," *IEEE Trans. Veh. Technol.*, vol. 61, no. 9, pp. 3825–3837, Nov. 2012.

[18] D. D. Wentzloff, "Pulse-Based Ultra-Wideband Transmitters for Digital Communication," Ph.D. dissertation, Mass. Inst. Technol., Cambridge, MA, USA, Jun. 2007.

[19] X. Dong, L. Jin, and P. Orlik, "A new transmitted reference pulse cluster system for UWB communications," *IEEE Trans. Veh. Technol.*, vol. 57, no. 5, pp. 3217–3224, Sep. 2008.

[20] D. D. Wentzloff and A. P. Chandrakasan, "Gaussian pulse generator for subbanded ultra-wideband transmitters," *IEEE Trans. Microw. Theory Techn.*, vol. 54, no. 4, pp. 1647–1655, Apr. 2006.

[21] F. R.-Mireles, "Signal design for ultra-wide-band communications in dense multipath," *IEEE Trans. Veh. Technol.*, vol. 51, no. 6, pp. 1517–1521, Nov. 2002.

[22] A. D. Angelis, M. Dionigi, R. Giglietti, and P. Carbone, "Experimental comparison of low-cost sub-nanosecond pulse generators," *IEEE Trans. Instrum. Meas.*, vol. 60, no. 1, pp. 310–317, Jan. 2011.

[23] F. R. -Mireles, "Performance of UWB *N*-orthogonal PPM in AWGN and multipath channels," *IEEE Trans. Veh. Technol.*, vol. 56, no. 3, pp. 1272–1285, May 2007.

[24] A. Cazzorla, G. D. Angelis, A. Moschitta, M. Dionigi, F. Alimenti, and P. Carbone, "A 5.6 GHz UWB position measurement system," *IEEE Trans. Instrum. Meas.*, vol. 62, no. 3, pp. 2538–2548, Mar. 2013.

[25] A. V. Oppenheim, A. S. Willsky, and I. T. Young, *Signals and Systems*. Englewood Cliffs, NJ, USA: Prentice-Hall, 1983.

[26] *R&S FSV Signal and Spectrum Analyzer Operating Manual*, Rohde & Schwarz GmbH & Co. KG, München, Germany, 2014.

[27] M. Abramowitz and E. I. Stegun, *Handbook of Mathematical Functions With Formulas, Graphs, and Mathematical Tables* (Applied Mathematics Series 55), 10th ed., U.S. Dept. Commerce, Nat. Bureau Stand., Dec. 1972.

[28] S. Wolfram, *The Mathematica Book*, 5th ed. Cambridge, U.K.: Cambridge Univ. Press, Aug. 2003.

Tamás István Krébesz (M'10) received the M.Sc. degree in electrical engineering from the Budapest University of Technology and Economics (BME), Budapest, Hungary, in 2007, where he is currently working toward the Ph.D. degree in electrical engineering with the Department of Measurement and Information Systems.

He is currently a University Lecturer with the BME. He was an Academic Visitor and Research Assistant with The Hong Kong Polytechnic University, Hong Kong, in 2009, 2012, and 2013 and with INSA-LATTIS Laboratory, Toulouse, France, in 2009 and 2010. He has been providing consulting service for multinational corporations (e.g., National Instruments, Continental, Enersys). His research and professional interests include ultrawide band radio, chaos communications, networking devices of embedded systems, and automated measurement systems providing traceability.

Mr. Krébesz received the Outstanding Young University Teacher Award from the Department of Measurement and Information Systems, BME, in 2015. He serves the IEEE-Hungary Section as Chair of Circuits, Systems, Computers Joint Chapter.

Géza Kolumbán (M'92–SM'98–F'05) received the M.Sc. and Ph.D. degrees in circuit theory from the Technical University of Budapest, Budapest, Hungary, in 1976 and 1990, respectively; the C.Sc. and D.Sc. degrees in telecommunications from the Hungarian Academy of Sciences, Budapest, in 1990 and 2004, respectively; and the Dr.habil degree from the Budapest University of Technology and Economics in 2005.

After his graduation, he spent 15 years in the professional telecommunications industry, where he developed microwave circuits and phase-locked loop (PLL)-based frequency synthesizers. Later, he was involved in many system engineering projects from an single-channel-per-carrier-type satellite telecommunication system to microwave terrestrial digital radio systems. After joining university education, he showed that chaos may exist in autonomous PLLs and established noncoherent chaotic communications as a brand new research direction. He developed differential chaos shift keying and frequency-modulated differential chaos shift keying: the most popular chaotic modulation schemes. Two of his papers, coauthored with Profs. M. P. Kennedy and L. O. Chua, have been ranked in top-cited IEEE TRANSACTIONS ON CIRCUITS AND SYSTEMS I: Regular Papers. He has been a visiting Professor and Researcher with UC Berkeley; PolyU and CityU in Hong Kong, University College Dublin and Cork, Ireland; École polytechnique fédérale de Lausanne, Lausanne, Switzerland; INSA-LATTIS Laboratory, Toulouse, France; and TU Dresden, Dresden, Germany. He has been providing consulting service for many companies from National Instruments to Samsung Advanced Institute of Technology. He is currently a Professor with the Faculty of Information Engineering and Bionics of Pázmány Péter Catholic University, Budapest, and is an Adjunct Professor with the School of Engineering, Edith Cowan University, Perth, Australia. His current research interests include software-defined electronics, analysis and computer simulation of complex systems, phase-locked loops, chaotic and ultrawide band radio communications, implementation of automated manufacturing lines, and automated testing systems.

Prof. Kolumbán received the IEEE Fellowship in 2005 for his contributions to the theory of "double sampled phase-locked loops and noncoherent chaotic communications." He served as an IEEE CAS Distinguished Lecturer during 2013–2014. He is on the Editorial Board of the *Elsevier DSP Journal* and serves as an Associate Editor for the IEEE TRANSACTIONS ON CIRCUITS AND SYSTEMS PART II and the *DCBIS-B Journal*.

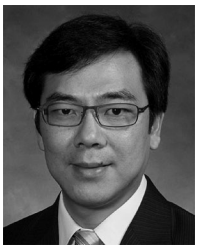

Chi K. Tse (M'90–SM'97–F'06) received the B.Eng. (Hons.) degree with first class honors in electrical engineering and the Ph.D. degree in electrical engineering from the University of Melbourne, Melbourne, Australia, in 1987 and 1991, respectively.

He is currently a Chair Professor with the Hong Kong Polytechnic University, Hong Kong, with which he served as the Head of the Department of Electronic and Information Engineering from 2005 to 2012. He is author/coauthor of 10 books, 20 book chapters, and more than 500 papers in research journals and conference proceedings, and holds five US patents.

Dr. Tse has received a number of research and industry awards, including the Best Paper Award from the IEEE TRANSACTIONS ON POWER ELECTRONICS in 2001; the Best Paper Award from the International Journal of Circuit Theory and Applications in 2003; two Gold Medals at the International Inventions Exhibition in Geneva in 2009 and 2013; and a number of recognitions by the academic and research communities, including honorary professorships from several Chinese and Australian universities; Chang Jiang Scholar Chair Professorship; IEEE Distinguished Lectureship; Distinguished Research Fellowship from the University of Calgary; Gledden Fellowship; and International Distinguished Professorship-at-Large from the University of Western Australia. While with the Hong Kong Polytechnic University, he received the President's Award for Outstanding Research Performance twice, the Faculty Research Grant Achievement Award twice, the Faculty Best Researcher Award, and several teaching awards. He serves and has served as the Editor-in-Chief for the IEEE TRANSACTIONS ON CIRCUITS AND SYSTEMS II (2016–2017), *IEEE Circuits and Systems Magazine* (2012–2015), *IEEE Circuits and Systems Society Newsletter* (since 2007), an Associate Editor for three IEEE Journal/Transactions, an Editor for *International Journal of Circuit Theory and Applications*, and is on the editorial boards of a few other journals. He also serves as panel member of the Hong Kong Research Grants Council and NSFC and as a member of several professional and government committees.

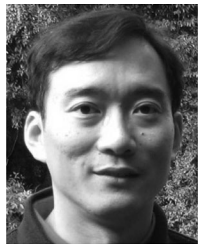

Francis C. M. Lau (SM'03) received B.Eng. (Hons.) degree and the Ph.D. degree both in electronic and electrical engineering from Kings College London, University of London, London, U.K.

He is a Professor and the Associate Head with the Department of Electronic and Information Engineering, The Hong Kong Polytechnic University, Hong Kong. His research interests include chaos-based digital communications, channel coding, cooperative networks, wireless sensor networks, applications of complex-network theories, and wireless communications. He is the coauthor of two research monographs—*Chaos-Based Digital Communication Systems* (Springer-Verlag, Heidelberg, Germany, 2003) and *Digital Communications with Chaos: Multiple Access Techniques and Performance Evaluation* (Elsevier, Oxford, U.K., 2007). He coholds two U.S. patents related to chaos-based communications and two other U.S. patents related to channel encoders/decoders. He has published more than 270 research papers, including more than 100 journal publications. Many of them appear in IEEE journals.

Dr. Lau has also served as the Technical Committee Program Member, Session Chair, and Reviewer of many international conferences and has served as an Associate Editor for several journals, including the IEEE TRANSACTIONS ON CIRCUITS AND SYSTEMS II (2004–2005), IEEE TRANSACTIONS ON CIRCUITS AND SYSTEMS I (2006–2007), and *IEEE Circuits and Systems Magazine* (2012–2015). His publications received the Best Paper Award at the International Conference on Advanced Technologies for Communications (2011 and 2015) and the Outstanding Paper Awards at the International Conference on Advanced Communication Technology (2012 and 2013). He has been a guest Associate Editor of the *International Journal of Bifurcation and Chaos* since 2010 and an Associate Editor of IEEE TRANSACTIONS ON CIRCUITS AND SYSTEMS II since 2016. He was also the Chair of the Technical Committee on Nonlinear Circuits and Systems, IEEE Circuits and Systems Society, from 2012 to 2013 and the cotrack Chair of the Nonlinear Circuits and Systems, 2010 IEEE International Symposium on Circuits and Systems.

Hairong Dong (M'12–SM'12) received the B.S. and M.S. degrees in automatic control and basic mathematics from Zhengzhou University, Zhengzhou, China, in 1996 and 1999, respectively, and the Ph.D. degree in general and fundamental mechanics from Peking University, Beijing, China, in 2002.

She is currently a Professor with the State Key Laboratory of Rail Traffic Control and Safety, Beijing Jiaotong University. She was a Visiting Scholar with the University of Southampton, Southampton, U.K., in 2006; the University of Hong Kong, Pokfulam, Hong Kong, in 2008; the City University of Hong Kong, Kowloon, Hong Kong, in 2009; the Hong Kong Polytechnic University, Kowloon, in 2010; and KTH Royal Institute of Technology, Stockholm, Sweden, in 2011, as well as the University of Birmingham, Birmingham, U.K., in 2013, and so on. Her research interests include stability and robustness of complex systems, control theory, intelligent transportation systems, automatic train operation, and parallel control and management for high-speed railway systems.

Prof. Dong is an Associate Editor of the IEEE TRANSACTIONS ON INTELLIGENT TRANSPORTATION SYSTEMS, *IEEE Intelligent Transportation Systems Magazine*, and *Acta Automatica Sinica* and is a Member of the IEEE Intelligent Transportation Systems Society and Chinese Automation Congress.